AUT Journal of Electrical Engineering
10.22060/EEJ.2026.24306.5679

Development and Control of High-Gain Triple Winding Max Gain BOOST Converter with Intelligent Walrus-RBFFIS MPPT for Photovoltaic Applications

J. Viswanatha Rao[1,*], R. Sundar[2], G. S. Satheesh Kumar[3], G. W. Martin[4]

[1]Department of Electrical and Electronics Engineering, VNR Vignana Jyothi Institute of Engineering & Technology, Hyderabad, India.
[2]Associate Professor, Department of Marine Engineering, AMET Deemed to be University, India.
[3]Associate Professor, Department of Electrical and Electronics Engineering, Erode Sengunthar Engineering College, Perundurai – 638057, India.
[4]Professor, Department of Electrical and Electronics Engineering, Marthandam College of Engineering and Technology, Tamilnadu-629177, India.
[*]Corresponding author E-mail: viswanatharao_j@vnrvjiet.in

Abstract:

Currently, the combination of Renewable Energy Sources (RES), particularly Photovoltaic (PV) systems, into power networks has grown in importance for sustainable energy generation. Therefore, this research develops the control approach for a high gain Triple Winding Max Gain Boost (TWMGB) converter incorporated with a Maximum Power Point Tracking (MPPT) controller for PV systems. The developed converter exploits a triple winding inductor structure to attain an improved voltage gain, making it appropriate for low voltage PV system needs effective step-up capability. An innovative MPPT control approach based on Walrus Optimization Algorithm (WOA) tuned Radial Basis Function Fuzzy Inference System (RBFFIS) is utilized to extract the upmost power from the PV array in dynamic ecological conditons. It assures fast convergence to the globalMPP and enahnces tracking accuracy even in partial shading scenarios. Moreover, the coordinated interaction among the TWMGB converter and adaptive control approach assures better performance interms of diminshed voltage stress and ripple. The performance of a system is applied via MATLAB/Simulink tool, demonstrating its adaptability and robustness with converter efficacy of 97.61%. The developed system offers a consistent and scalable solution for advanced PV based power systems, contributing to sustainable energy conversion and utilization.

Uncorrected Proof

AUT Journal of Electrical Engineering
10.22060/EEJ.2026.24306.5679

Keywords:

PV system, TWMGB converter, WOA, RBFFIS MPPT.

1. Introduction

The fossil fuels that are exploited to produce power, which is not good for the environment and contributes significantly to climate change. Additionally, a global energy crisis has been predicted as a result of decades of extensive fossil fuel exploitation [1, 2]. One sustainable way to address the need for electricity is through microgrids. A microgrid function independently or in conjunction with the grid to supply energy to a particular area, such as a community, campus or industrial facility. The most appropriate and cost-effective method of supplying electricity is a microgrid that is powered by Renewable Energy Sources (RESs) [3]. Renewable energy technologies are seen as sustainable substitutes for fossil fuels and offer a cleaner, more environmentally friendly source of electricity [4, 5]. RESs include biomass, PV, small hydro, solar thermal, geothermal, wind and biogas [6]. Technologies based on renewable energy, especially solar photovoltaic and wind energy conversion systems, are booming because they are widely accessible and offer a sustainable and environmentally pleasant way to meet future power needs [7].

For many energy systems, whether centralized or decentralized, developing PV technologies are the chosen low-carbon alternative due to their abundance, ease of use and minimal environmental impact. Nevertheless, as PV penetration keeps rising, the power grid finds it challenging to use large amounts of PV energy due to the unpredictability and instability of PV generation [8]. The DC-DC converters are necessary to overcome this issues that includes Boost converter [9] overcome the unpredictability in solar panel output. Low voltage gain, fewer voltage ripples, temperature dependency, maximum voltage stress over the switches and massiveness are some of these converters' drawbacks. Applications that demand greater output voltage levels from low input voltages are benefit from the coupled inductor-based Boost converter, which is demonstrated in [10]. It allows for effective coupling and substantially higher step-up

Uncorrected Proof

voltages. However, the large voltage spikes brought on by leakage inductance is one of the major problems with coupled inductor converters. A large voltage gain at a moderate duty cycle, minimal switching losses and better efficacy are all provided by the extended boost converter in [11]. It is expanded to provide maximum voltage gains by enhancing the number of cascading cells. However, because of the extra components, it has a more complicated design, larger output voltage ripple and higher prices.

In order to reduce the intricacy of the control circuit for getting a static DC voltage at the output side for flexible input loads or voltages, a boost converter based on switched capacitors and inductors is invented in [12]. Nevertheless, because of the high-frequency operation, it frequently shows higher switching losses and conduction losses. A quadratic buck-boost converter [13] has high efficiency, compact size and shared source and load characteristics. However, it indicate reduced efficiency as a result of frequency loss in diodes and hysteresis and eddy current loss in inductors. In [14], the three-winding coupled-inductor -boost converter is exploited that has a maximum voltage conversion ratio. Nevertheless, the reliance on the coupled inductor design that lead to improved susceptibility to failure within the converter. The Two winding coupled inductor has the reduced ripple current and offer galvanic isolation among the windings. However, it enhances the output voltage ripple because of the current ripples from both windings [15].

Henceforth, this research develops a high-gain triple winding max gain boost converter for enhancing the PV voltage into required level. To track the MPP of PV under various irradiance profiles, a variety of MPPT approaches have been introduced [16, 17]. It includes ANN [18], Fuzzy [19] and ANFIS [20, 21] that have higher accuracy, higher precision and stability around the maximum power point, effectively reduces tracking errors. However, that approaches are time consuming, uncertainties in input data and higher complexity. Thus, the RBFFIS-MPPT is utilized for tracking highest power from PV system and is performance is enhanced by an optimization algorithm, comprising Particle Swarm Optimization (PSO) [22] performs well in exploring large search spaces. However, the convergence rate is slow as particles oscillate around the best-found solution.

Uncorrected Proof

The Gray Wolf Optimization (GWO) is presented in [23] that exhibits a quick convergence rate, permitting it to efficiently detect optimal solutions in several optimization problems. Nevertheless, GWO has fewer parameters compared to some algorithms, unsuitable settings of these parameters are still adversely influence its performance. Firefly algorithm [24] is suitable for solving highly multimodal and non-linear optimization problems. Nonetheless, the FA is get trapped in local optima due to its reliance on current performance. An Artificial Bee Colony [25] algorithm exhibits strong exploration capabilities, as it efficiently explores the solution space. However, ABC algorithm is struggle with exploitation, it sometimes fail to efficiently refine solutions after initial exploration. The Zebra optimization algorithm is presented in [26] that has fewer parameters and easy implementation but suffers from premature convergence and local optima entrapment. Pelican optimization algorithm has the fast convergence rate and efficient exploitation and exploration capabilities. However, it has premature convergence and diversity problems in the population [27]. To overcome these difficulties, the walrus optimized RBFFIS-MPPT algorithm is exploited. The main contribution are,

- Implementing high-gain triple winding max gain boost converter for enhancing the PV system's voltage with maximum efficacy.
- Incorporating RBFFIS-MPPT for peak power extraction and is parameters are fine-tuned by WOA.

2. Proposed Methodology

Fig. 1 represents the block diagram of proposed work. Initially, the PV system acquires the solar energy and transforms it into power. Then, the output of PV system is delvers into TWMGB converter that utilizes the magnetic coupling and multiple inductor windings to attain a better voltage gain.

Uncorrected Proof

10.22060/EEJ.2026.24306.5679

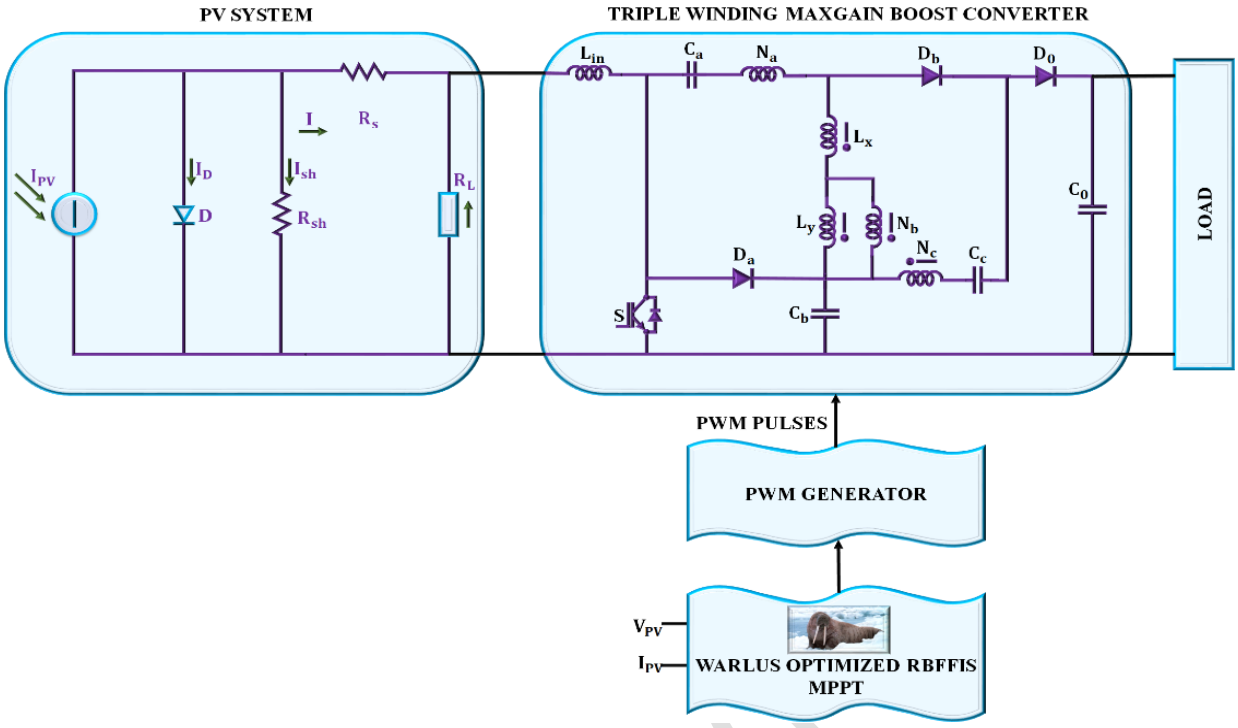

Fig. 1. Block diagram of proposed work

To assure optimum power extraction from PV panel, the Walrus optimized RBFFIS MPPT controller is exploited. It integrates the fast learning and nonlinear mapping ability of RBFFIS with global search ability of WOA that simulates the group mitigation and collision avoidance characteristics of walruses. It constantly processes the real time values of V_{PV} and I_{PV} to estimate the optimal duty cycle for converter operation. This duty cycle is then transformed into high frequency switching pulses by the PWM generator. It assures that the converter constantly function at the point of highest power transfer from the PV panel, improving overall system performance. It adapts dynamically to environmental changes, making it better for applications like microgrids, electric vehicle charging and off-grid power systems.

2-1- PV System

The PV system alters solar into power. Its current and voltage is detected by the amount of series and parallel cells. The PV system's circuit is displayed in Fig. 2. The PV panel's general equation is,

Uncorrected

10.22060/EEJ.2026.24306.5679

$$I_{pv} = I_{sh} - I_d - I_p \tag{1}$$

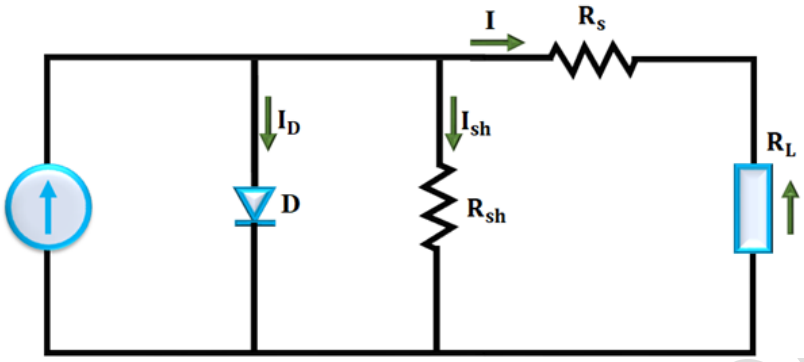

Fig. 2. Circuit of PV system

Where, current flowing over the parallel resistance is denoted by I_p, current passing over the diode is I_d and is,

$$I_0\left[\exp\left(V + \frac{IR_S}{\alpha V_T}\right) - 1\right] = I_d \tag{2}$$

$$I_p = \left(V + \frac{IR_S}{R_p}\right) \tag{3}$$

By applying Expression (2) and (3) in Expression (1),

$$I_{pv} = I_{sh} - I_0\left[\exp\left(V + \frac{IR_S}{\alpha V_T}\right) - 1\right] - \left(V + \frac{IR_S}{R_p}\right) \tag{4}$$

Then, the PV system's low voltage is improved by a triple winding max gain boost converter and its operation is discussed below.

2-2- High-Gain TWMGB Converter

The C_b and D_a serve as the passive clamp circuit in the developed converter. Only the voltage of the capacitor C_b provide voltage stress on the switch. At the converter's input stage, the inductor Lin controls input power

Uncorrected Proof

10.22060/EEJ.2026.24306.5679

and lowers input current ripple. The circuit of the TWMGB converter is revealed in Fig. 3. Fig. 4 shows the switching waveform of the developed converter.

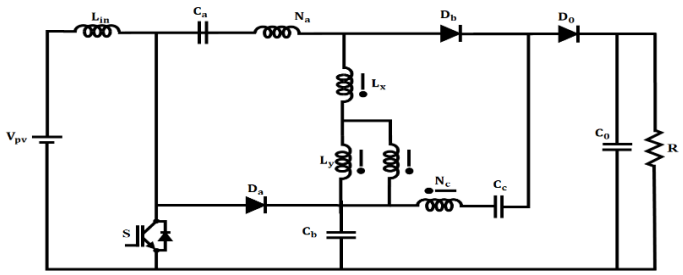

Fig. 3. Circuit of TWMGB Converter

Mode I:

Here, S is active in the first operating mode, as seen in Fig. 5(a). The input voltage charges the inductorL_{in}. The D_c is active to pass the current of the coupled inductor's third winding, while $D_a$and D_b are inactive. The same diode $D_c$current is exploited to charge the output capacitor. When the coupled inductor's third winding's current reverses, this operating state is ended.

Mode II:

The third winding of the connected inductor's current direction shifts over the time period. Consequently, $D_b$is ON and $D_c$is OFF, as revealed in Fig. 5(b). In this stage, $C_a$and $C_b$charge the magnetizing inductorL_y. To source the load, the output capacitor is discharged. The current passing over the coupled inductor's third winding charges the capacitor C_c . When the power switch is inactive , this mode is ended.

Mode III:

The switch S is inactive during this stage . As a result, the inductor current is conducted by turning on the diodeD_a. The passive clamp circuit is operational in this mode and the power switch's voltage stress is restricted to VC_b. This period of time is short and ends when the diode $D_b$is inactive and the third winding coupled inductor's current is reversed, as indicated in Fig. 5(c).

Mode IV:

Uncorrected Proof

10.22060/EEJ.2026.24306.5679

The diode $D_c$is activated during this time. As a result, the output capacitor is charged by the connected inductor's third winding current, as represented in Fig. 5(d). The C_a releases the magnetizing inductor. As soon as $D_a$is switched off, this mode is terminated.

Mode V:

When the inductor current and the coupled inductor's second winding current are equal, this mode is initiated, as revealed in Fig. 5 (e). Consequently, the diode $D_a$is off. The C_b and $C_O$are charged while $C_a$and C_c are discharged. When the switching period is over, this stage is concluded and the S is turned back on during the subsequent switching cycle. Since stages I and III are small, they are disregarded. The voltage across L_{in} and the coupled inductor's magnetizing inductor in mode 2 by applying KVL is,

$$V_{Lin} = V_{PV} \tag{5}$$

Here, the input voltage is similar to voltage of L_{in}.

$$V_{Ly} = \frac{1}{\frac{N_b}{N_a} - 1}\left(V_{Ca} - V_{Cb}\right) \tag{6}$$

$$V_{Ly} = \frac{V_{Cc}}{\frac{N_c}{N_a} + 1} \tag{7}$$

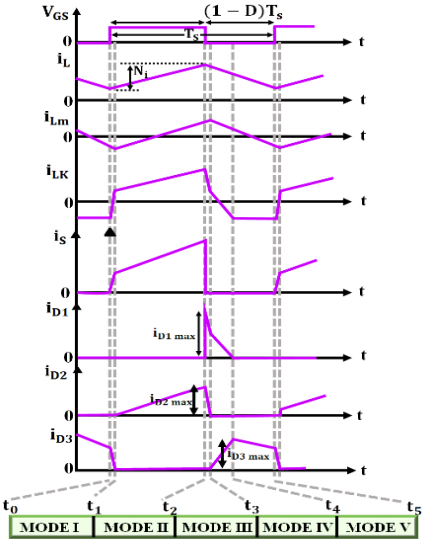

Uncorrected Proof

Fig. 4. Switching waveform of TWMGB Converter

The voltages of the inductors in mode 4 are,

$$V_{PV} - V_{Cb} = V_{Lin} \tag{8}$$

$$\frac{V_{Ca}}{\frac{N_b}{N_a} - 1} = V_{Ly} \tag{9}$$

$$\frac{1}{\frac{N_c}{N_a} + 1}\left(V_{Cc} + V_{Cb} - V_o\right) = V_{Ly} \tag{10}$$

By applying the KVL in mode 5,

$$\left(V_{Cb} + V_{Cc} - V_o\right)\frac{1}{\frac{N_c}{N_a} + 1} = V_{Ly} \tag{11}$$

$$\left(\frac{N_b}{N_a} - 1\right)V_{Ly} + V_{Lin} = V_{Ca} - V_{Cb} + V_{PV} \tag{12}$$

The voltage of the inductor L_{in} in mode 5 is,

$$V_{Lin} = V_{PV} - V_{Cb} \tag{13}$$

Uncorrected Proof

10.22060/EEJ.2026.24306.5679

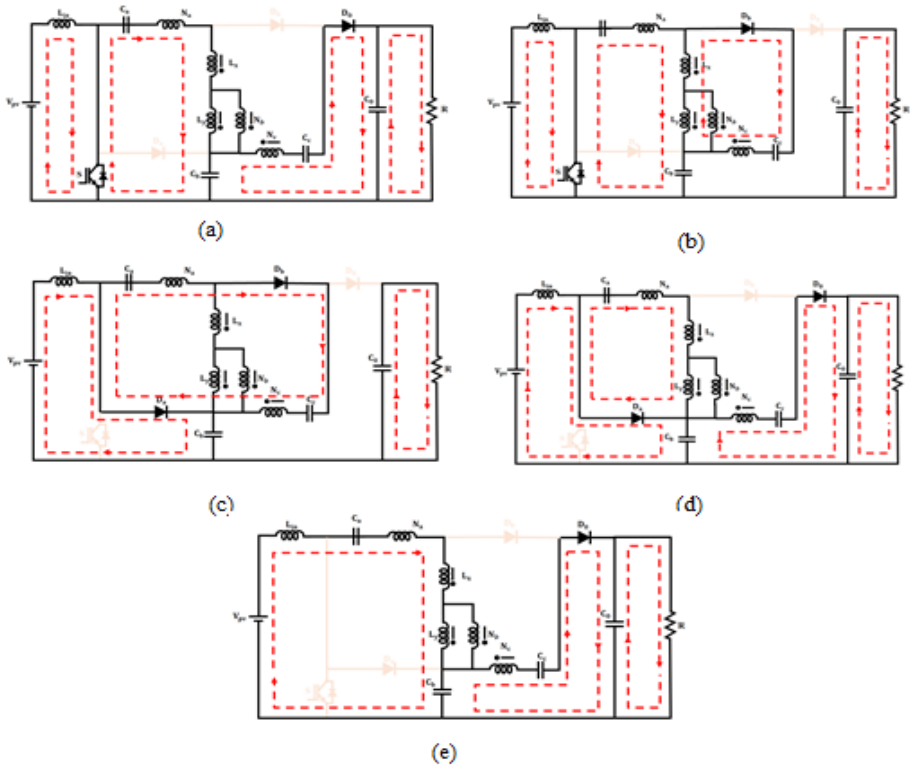

Fig. 5. TWMGB converter's (a) stage 1 (b) stage 2 (c) stage 3 (d) stage 4 (e) stage5

The voltage of the C_b is,

$$V_{Cb} = \frac{V_{PV}}{1-D} \tag{14}$$

The magnetizing inductor's voltage in mode 5,

$$\frac{V_{Ca}}{\frac{N_b}{N_a}-1} = V_{Ly} \tag{15}$$

$$\frac{DV_{PV}}{1-D} = V_{Ca} \tag{16}$$

The voltage of C_c is,

$$V_{Cc} = \frac{N_a + N_c}{N_a - N_b} V_{PV} \tag{17}$$

Uncorrected

10.22060/EEJ.2026.24306.5679

$$M = \frac{V_O}{V_{PV}} = \frac{\left(1 + \frac{N_a + N_c}{N_a - N_b}\right)}{1 - D} \tag{18}$$

Loss Analysis

The RMS values are,

$$\sqrt{\frac{1}{T_S}\int_0^{d_4 T_S}\left[\left(1 - \frac{t}{d_4 T_S}\right)\right]^2 i_{Da}^{max} dt} = I_O\sqrt{\frac{2M}{3}} = I_{Da}^{RMS} \tag{19}$$

$$\sqrt{\frac{1}{T_S}\int_0^{DT_S}\left(\frac{i_{Db}^{max}}{DT_S}t\right)^2 dt} = 2I_O\sqrt{\frac{1}{3D}} = I_{Db}^{RMS} \tag{20}$$

$$\sqrt{\frac{1}{T_S}\left[\int_0^{d_4 T_S}\left(\frac{i_{Dc}^{max}}{d_4 T_S}t\right)^2 dt = \int_{d_4 T_S}^{T_S}\left(i_{Dc}^{max}\right)^2 dt\right]} = I_{Dc}^{RMS} \tag{21}$$

$$i_{Dc}^{max}\sqrt{1 - D - \frac{4M}{3}} = I_{Dc}^{RMS} \tag{22}$$

The total power loss is,

$$r_{Da} I_{Da}^{rms2} + r_{Db} I_{Db}^{rms2} + r_{Dc} I_{Dc}^{rms2} = P_{rD} \tag{23}$$

The power loss is,

$$P_{VF} = \left(V_{Fa} + V_{Fb} + V_{Fc}\right) I_O = \frac{\left(V_{Fa} + V_{Fb} + V_{Fc}\right) P_O}{V_O} \tag{24}$$

The switch current's RMS value is,

$$I_S^{RMS} = \sqrt{\frac{1}{T_S}\int_0^{DT_S}\left[I_{Lin} + \frac{i_S^{max} - I_L}{DT_S}t\right]^2 dt} \tag{25}$$

$$I_S^{RMS} = \sqrt{DI_O\sqrt{M^2 + \frac{2MN_c}{N_b D}} + \frac{4N_c^2}{3N_b^2 D^2}} \tag{26}$$

The switching loss is,

Uncorrected Proof

$$f_S C_S V_S^2 = f_S C_S \left(\frac{V_{PV}}{1-D} \right) =^2 P_S \tag{27}$$

Here, the switching frequency is denoted as f_S and switch's parasitic capacitance is C_S. Thus, the switch's power loss is,

$$P_{SW}^{Total} = f_S C_S \left(\frac{V_{PV}}{1-D} \right)^2 + I_S^{RMS2} r_S \tag{28}$$

The power loss is,

$$P_L = r_L I_L^{RMS2} = r_L M^2 I_O^2 \tag{29}$$

The main side of the coupled inductor's current is,

$$i_{Na}^{RMS} = \frac{N_c}{N_a} \begin{cases} I_{Db}^{RMS} 0 < t < DT_S \\ I_{Dc}^{RMS} DT_S < t < T_S \end{cases} \tag{30}$$

The coupled inductor's overall power loss is,

$$r_{C1} I_{Na}^{RMS2} = P_{Coupled-Inductor} \tag{31}$$

Where, the coupled inductor's total equivalent resistance is C_1.The capacitor currents are,

$$\frac{N_c}{N_b} i_{Cc} = i_{Ca} = \begin{cases} -\frac{N_b}{N_c} i_{Db} 0 < t < DT_S \\ \frac{N_b}{N_c} i_{Dc} DT_S < t < T_S \end{cases} \tag{32}$$

$$i_{Cb} = \begin{cases} -i_{Db\left(1+\frac{N_a}{N_c}\right)} 0 < t < DT_S \\ \frac{N_a}{N_c} i_{Dc} + i_{Da} DT_S < t < T_S \end{cases} \tag{33}$$

The RMS values of the capacitors are,

Uncorrected Proof

10.22060/EEJ.2026.24306.5679

$$I_{Ca}^{RMS}=\frac{N_c}{N_a}i_{Cc}^{RMS}+\frac{N_b}{N_c}I_O\sqrt{\frac{4}{3D}+\frac{1-D-\frac{4M}{3}}{1-D-\frac{2}{M}}} \tag{34}$$

$$I_{Cb}^{RMS}=I_O\sqrt{M\left[\frac{14\left(\frac{N_a}{N_c}\right)^2+11\left(\frac{N_a}{N_c}\right)+2}{3\left(\left(\frac{N_a}{N_c}\right)+1\right)^2}\right]+\frac{4\left(\left(\frac{N_a}{N_c}\right)+1\right)^2}{3D}} \tag{35}$$

The capacitor loss is,

$$r_{Ca}I_{Ca}^{RMS2}+r_{Cb}I_{Cb}^{RMS2}+r_{Cc}I_{Cc}^{RMS2}=P_C \tag{36}$$

Subsequently, the uppermost power from PV system is extracted by utilizing RBFFIS MPPT controller and its performance is enhanced by WOA.

2-3- Walrus Optimized RBFFIS MPPT Controller

For tuning the parameters of RBFFIS based MPPT, the WOA is exploited for detecting the optimal parameter set that maximizes the output power from a PV system. The initial phase of WOA initiates with the random generation of population of walruses, where each walrus indicates a potential candidate solution to the optimization issue. These candidate solutions are encodes as vectors in population matrix as,

$$X=\begin{bmatrix} & & & & \\ x_{1,1} & \cdots & x_{1,J} & \cdots & x_{1,m} \\ \vdots & \ddots & \vdots & \iddots & \vdots \\ x_{i,1} & \cdots & x_{i,j} & \cdots & x_{i,m} \\ \vdots & \ddots & \vdots & \iddots & \vdots \\ x_{N,1} & \cdots & x_{N,j} & \cdots & x_{N,m} \end{bmatrix}_{N\times m} \tag{37}$$

Where, the number of walruses are denoted by N, the number of parameters to be tuned in the RBFFIS MPPT controller is m and j^{th} decision variable is $x_{i,j}$ suggested by i^{th} walrus. Each walrus vector X_i is

Uncorrected Proof

10.22060/EEJ.2026.24306.5679

estimated utilizing the objective function that quantifies the quality of MPPT. The objective function F_i for i^{th} walrus is,

$$F = \begin{bmatrix} \\ F(X_1) \\ \vdots \\ F(X_i) \\ \vdots \\ F(X_N) \end{bmatrix}_{N\times 1} \tag{38}$$

Where, the objective function vector is indicated by F. The objective function is developed to enhance the output power from the PV system or diminish the error among actual and reference power. As iterations proceed, the WOA updates the population based on the characteristics of walrus. In each iteration, the walrus population is updated to explore better configurations of the RBFFIS by adjusting the spreads, centers and output weights of the radial basis functions. Subsequently, the WOA guides the optimization process to evolve the RBFFIS parameters that result in highly accurate and MPPT control, particularly in varying environmental conditions. This initialization stage forms the basis for the iterative optimization process in WOA, assuring the RBFFIS controller track the MPP with robustness and high precision. In the exploration phase, the WOA mimics the natural foraging characteristics of walruses to explore the search space for optimal solutions.

Uncorrected Proof

10.22060/EEJ.2026.24306.5679

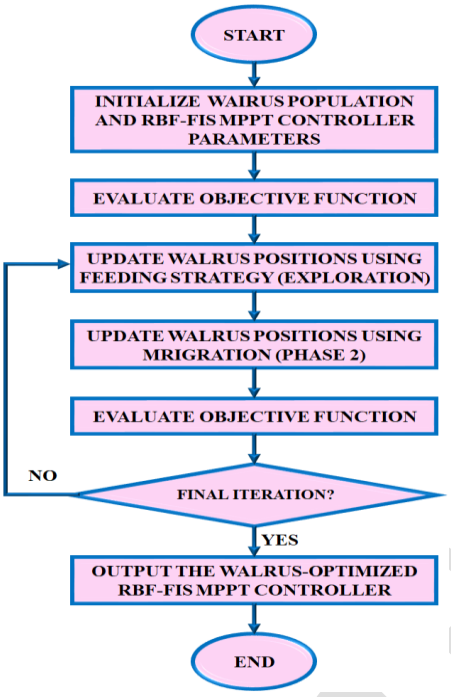

Fig. 6. Flowchart of Walrus optimized RBFFIS MPPT controller

Each walrus indicates a parameter configuration for the RBFFIS, comprising the widths and centers of the Gaussian functions and rule weights. To update the position of X_i , a new candidate position is generated by,

$$x_{i,j}^{P1} = x_{i,j} + rand_{i,j}.\left(SW_j - I_{i.j}.x_{i,j}\right) \tag{39}$$

Where, random variable is represented by $rand_{i,j}$, best solution's j^{th} parameter value is SW_j, $I_{i.j}$ are integers selected randomly among 1 or 2. It assures the candidate RBFFIS configurations, averting premature convergence to local optima. If the new configuration results in a better objective function value than the current one is replaced by,

$$X_i = \begin{cases} X_i^{P1}, F_i^{P1} < F_i \\ X_i, \quad else \end{cases} \tag{40}$$

This iterative update improves the global search ability of WOA and assures that the RBFFIS parameters are gradually refined towards attaining optimal MPPT performance. This stage tunes the RBFFIS MPPT

Uncorrected Proof

10.22060/EEJ.2026.24306.5679

controller to generate a duty cycle output that aligns with the MPP, under changing conditions. In the Migration phase, the WOA mimics the seasonal migration characteristics of Walruses that relocate to new habitats in search of more favourable conditions. This metaphor is employed in the algorithm to improve exploration and diversity by repositioning candidate solutions to new areas in the search space. This phase allows broader refinement of the RBFFIS parameters like the centers and spreads of Gaussian functions and output weights, assuring that the system is not prematurely converge to local optima and continues seeking better parameter configurations. Each Walrus representing a complete set of RBFFIS parameter, migrate towards the position of another randomly selected Walrus from the population. This migration replicates a shift in parameter space solution toward more promising regions, guided by comparative quality of other solutions. The new generation is generated by,

$$x_{i,j}^{P2} = \begin{cases} x_{i,j} + rand_{i,j}.\left(x_{k,j} - I_{i,j}.x_{i,j}\right), F_k < F_i \\ x_{i,j} + rand_{i,j}.\left(x_{k,j} - x_{i,j}\right), else \end{cases} \quad (41)$$

Here, new candidate solution's decision variable is indicated by $x_{i,j}^{P2}$, corresponding variable from k^{th} walrus is $x_{k,j}$, random variable is $rand_{i,j}$ and $I_{i,j}$ introduces the randomness in step size to enhance exploration ability. After developing this new position, its efficacy is estimated according to the objective function. The candidate solution is updated as,

$$X_i = \begin{cases} X_i^{P2}, & F_i^{P2} < F_i \\ X_i, & else \end{cases} \quad (42)$$

This phase assures that the WOA continues to balance local and global search, enabling the RBFFIS MPPT controller to evolve toward an optimal set of parameters. The dynamic adaptation of each walrus to potentially better solutions diversifies the populations and evades premature convergence. In the exploitation phase, the defensive characteristics of walruses when they encounter natural predators. This biological characteristics is changed into a local search that detects the search around each walrus's present position to fine-tune the better solutions. Here, the new position is computed as,

Uncorrected Proof

10.22060/EEJ.2026.24306.5679

$$x_{i,j} + \left(lb^{t}_{local,j} + \left(ub^{t}_{local,j} - rand.lb^{t}_{local,j} \right) \right) = x^{P3}_{i,j} \tag{43}$$

The local bounds $lb^{t}_{local,j}\ and\ ub^{t}_{local,j}$ are exploited to constrain the movement of the search within a particular neighbourhood is,

$$\text{Local bounds}: \begin{cases} lb^{t}_{local,j} = \dfrac{lb_j}{t} \\ ub^{t}_{local,j} = \dfrac{ub_j}{t} \end{cases} \tag{44}$$

Where, current iteration index is denoted by t, j^{th} variable's global upper and lower bounds are $ub_j\ and\ lb_j$. This assures that the neighbourhood radius shrinks over successive iterations, shifting the search focus from global exploration to precise local refinement. The newly generated RBFFIS configuration X_i^{P3} is evaluated utilizing the objective function that measures the MPPT performance, based on diminishing the tracking error or maximizing the output power. Then, the new position is updated as,

$$X_i = \begin{cases} X_i^{P3}, & F_i^{P3} < F_i \\ X_i, & else \end{cases} \tag{45}$$

It enables the WOA to conduct an intensive local search around high-quality solutions, thereby fine tuning the RBFFIS controller to enhance MPPT performance. Through this exploitation approach, the WOA assures the RBFFIS parameters are improved with enhancing precision, enabling the controller to constantly produce an ideal duty cycle for the developed converter. Then, each Walrus is constantly refined via these 3 behaviours across multiple iterations up to a predefined stopping criterion is met. The outcome is a very effective and robust MPPT approach that enhances power extraction from the PV array, reduces energy losses and improves overall system reliability.

3. Result and Discussion

Uncorrected Proof

10.22060/EEJ.2026.24306.5679

This section offers various simulation outcomes that confirm the efficacy of the developed TWMGB converter with WOA based RBFFIS MPPT controller under distinct weather conditions in MATLAB/Simulink tool. The specification of parameters is depicted in Table 1.

Table 1 Specification of parameters

Parameters	Specification
PV system	
Total Power	10K W
Panel's peak power	250 W
Current (Short circuit)	8.95 A
Maximum Peak Voltage	
Voltage (Open circuit)	37.25V
Maximum Peak Current	8.35 A
N_P	11
N_S	4
TWMGB converter	
C_a, C_b and C_c	22 µF
L_{in}	4.7mH
L_x, L_y	45mH, 700mH
C_O	2200 µF
Switching frequency	10kHz

Case 1: Steady State Condition

Uncorrected Proof

10.22060/EEJ.2026.24306.5679

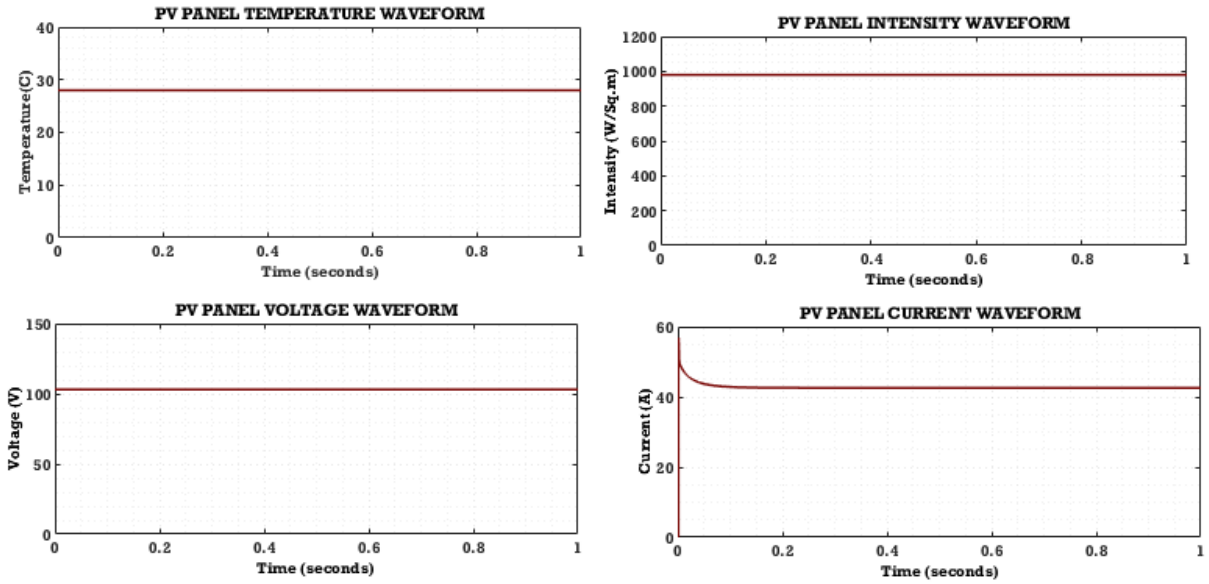

Fig. 7. Characteristics of solar panel

The characteristics of solar panel in steady state condition is presented in Fig. 7. The temperature is continued a steady value of $28℃$ while the intensity is sustained at $1000(W/Sq.m)$ in the complete system. Similarly, the voltage and current of PV system is settled at $110\,V$ and $42\,A$ (based on the temperature and intensity) without oscillations all over the system.

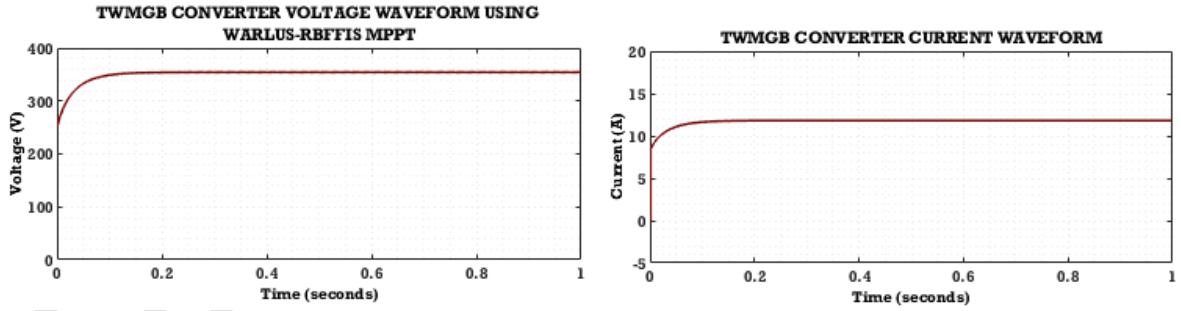

Fig. 8. Output waveforms of TWMGB converter

Based on this input voltage and current, the boosted output voltage is varied that is discussed in Fig. 8**.** Here, the output voltage is initially changed and is settled at $375\,V$ with little distortions. Subsequently, an output current is slowly changed and maintained at $12\,A$ without oscillations throughout the system.

10.22060/EEJ.2026.24306.5679

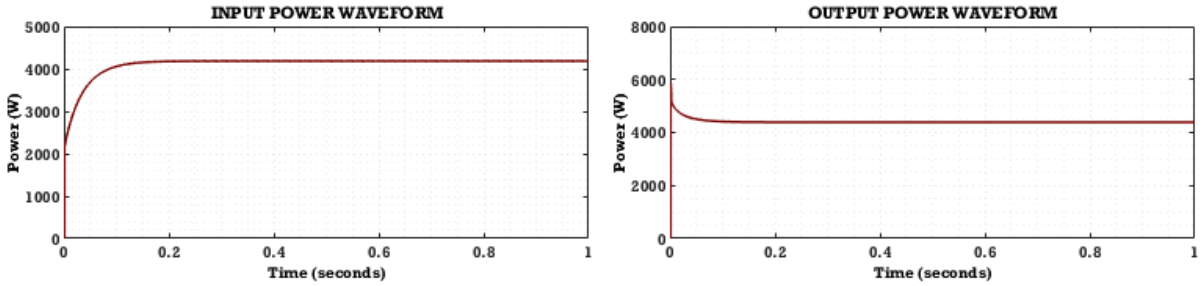

Fig. 9. Waveforms of power

Input and output waveforms of power is represented in Fig. 9. The input power is gradually raised and is stabilized at $4200\,W$ in the entire system. Consequently, an output power is reduced and maintained at $4100\,W$ without oscillations throughout the system.

Case 2: Varying condition

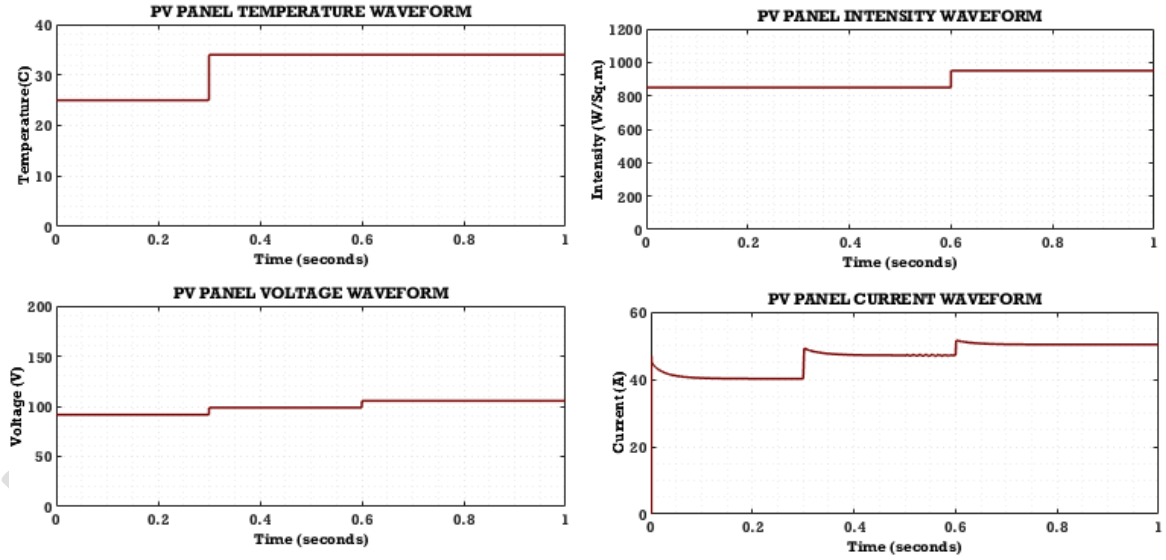

Fig. 10. Behaviour of solar panel (Case 2)

Fig. 10 indicates the behaviour of PV system in changing temperature and intensity condition. The temperature is changed in the beginning and is enhanced to steady value of 35℃ with no changes and

10.22060/EEJ.2026.24306.5679

intensity is also varied and sustained at $970(W/Sq.m)$ deprived of oscillations. The voltage of PV is varied slowly and maintained at $110\,V$ and current of PV is randomly varied and stabilized at $50\,A$.

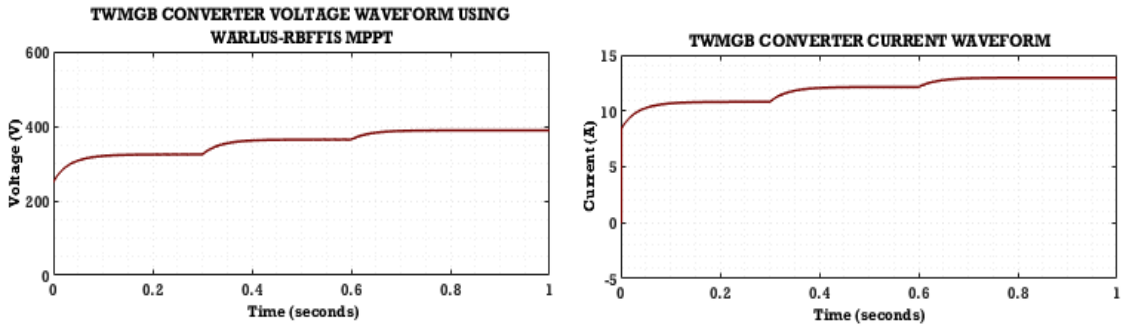

Fig. 11. Output waveforms of TWMGB converter

An output waveforms of TWMGB converter is depicted in Fig. 11. The TWMGB converter's output voltage is arbitrarily varied and maintained at $390\,V$ without distortions. Also, an output current is altered in the initial stage and sustained at $13\,A$.

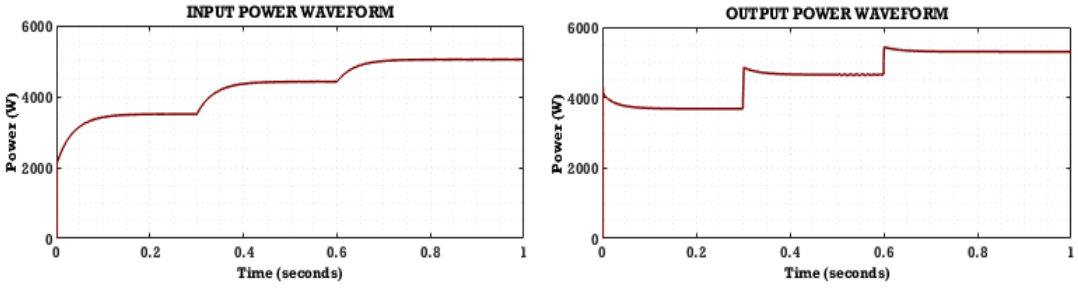

Fig. 12 Waveforms of power

Fig. 12 reveals the input and output waveforms of power. An input power is varied in the starting stage and is stabilized at $5000\,W$ and output power is changed randomly and it sustained at $4900\,W$ without variations.

10.22060/EEJ.2026.24306.5679

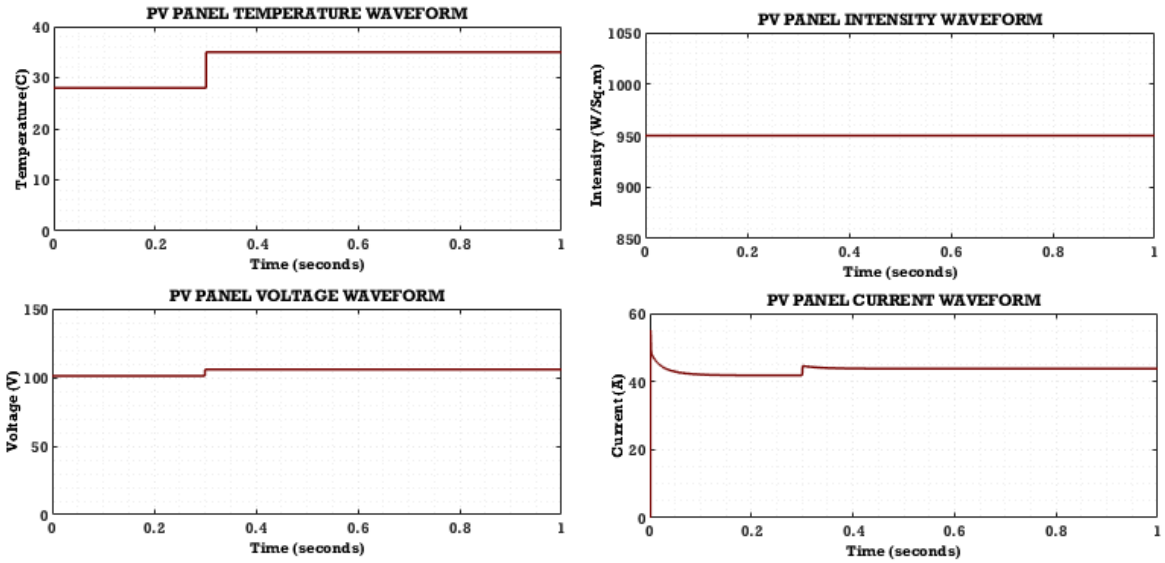

Fig. 13. Waveform of solar panel (Case 3)

The waveform of PV at fluctuating temperature and constant irradiation condition is represented in Fig. 13. In this condition, the temperature is varied and stabilized at 35℃ and persistent intensity of $950(W/Sq.m)$ is sustained in the system. The PV panel voltage is slowly raised in the initial stage and settled at $110\,V$. Also, the PV panel current is arbitrarily altered initially and continued at $45\,A$ in the system.

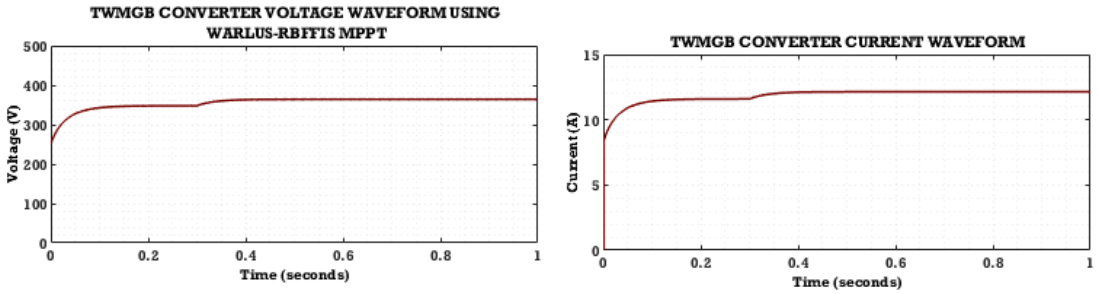

Fig. 14. Output waveforms of TWMGB converter

Fig. 14 presents an output waveforms of TWMGB converter. The TWMGB converter's output voltage with Walrus RBFFIS MPPT has initial changes and is maintained at $350\,V$ all over the system. The output current is randomly changed and sustained at $12\,A$ without distortions.

10.22060/EEJ.2026.24306.5679

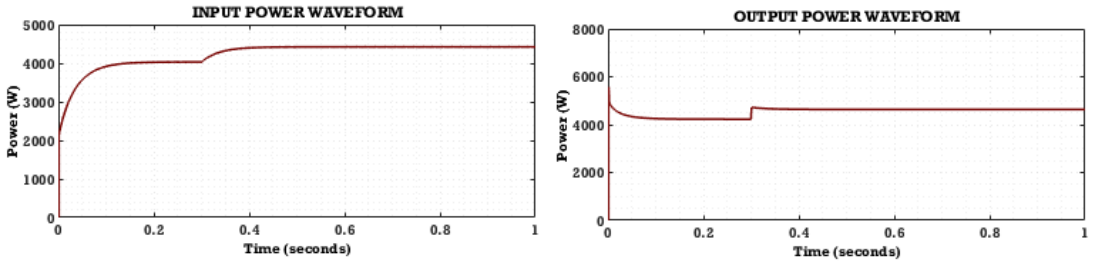

Fig. 15. Waveforms of power

The input and output waveforms of power is revealed in Fig. 15. An input power is slowly raised and settled at $4500\ W$ throughout the system. Then, an output power is gradually raised and maintained at $4400\ W$ without oscillations.

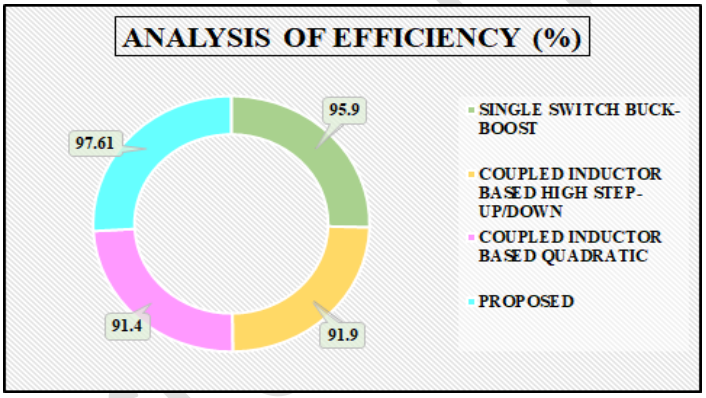

Fig. 16. Comparison of efficiency

Fig. 16 represents the comparison of efficiency for single switch Buck-Boost (95.9%) [28], Coupled inductor based high step-up/down (91.9%) [29], Coupled inductor based Quadratic (91.4 %) [30] and developed converter. Here, the developed converter has the maximum efficacy of 97.61%, demonstrating its improved ability in power conversion applications.

Uncorrected Proof

10.22060/EEJ.2026.24306.5679

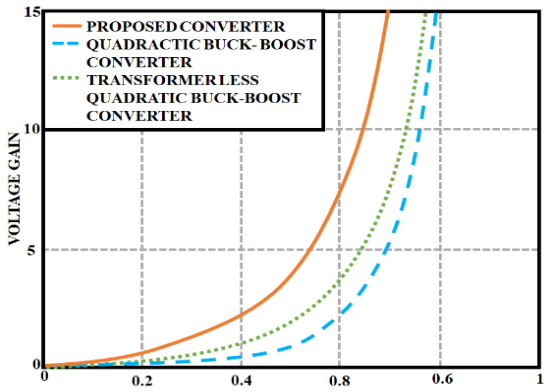

Fig. 17. Analysis of voltage gain

Fig.17 shows an analysis of voltage gain for Quadratic Buck-Boost [31], Transformer less Quadratic Buck-Boost [32] and developed converter that attains higher gain than other approaches. The Quadratic Buck-Boost converter has a moderate gain that enhances non-linearity with improving duty cycles while the Quadratic Buck-Boost without Transformer has better performance than Quadratic Buck-Boost converter. The TWMGB converter is appropriate for PV applications where maximizing energy extraction under variable irradiance conditions is vital.

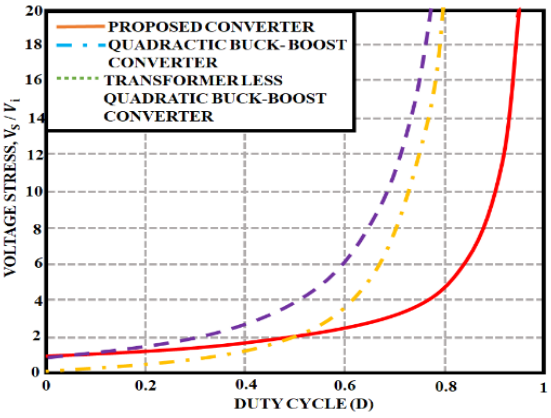

Fig. 18. Analysis of voltage stress on the switches

An analysis of voltage stress on the switches for Quadratic Buck-Boost [31], Transformer less Quadratic Buck-Boost [32] and developed converter is revealed in Fig. 18. The TWMGB converter has bottommost voltage stress, denoting diminished stress on switch and improved reliability. On the other hand, the

Uncorrected Proof

10.22060/EEJ.2026.24306.5679

Quadratic Buck-Boost and Transformer less Quadratic Buck-Boost converter has maximum voltage stress at higher duty cycles. Thus, the developed converter is more effective and sustainable for long-term deployment in RES.

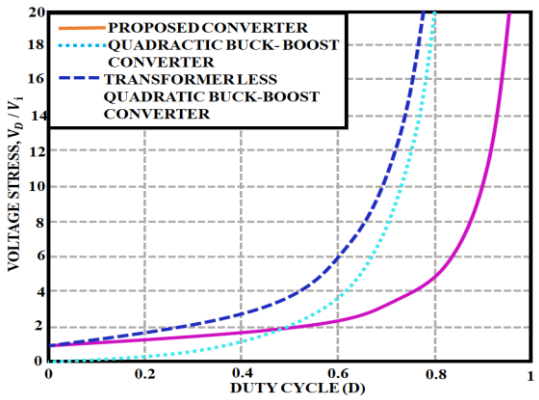

Fig. 19. Analysis of voltage stress on the diodes

The analysis of developed converter with for Quadratic Buck-Boost [31] and Transformer less Quadratic Buck-Boost [32] converter interms of voltage stress on the diodes is indicated in Fig. 19. The Quadratic Buck-Boost and Transformer less Quadratic Buck-Boost converter has higher voltage stress on diode. The developed converter have lesser voltage stress on the diodes that improves component durability and thermal efficacy.

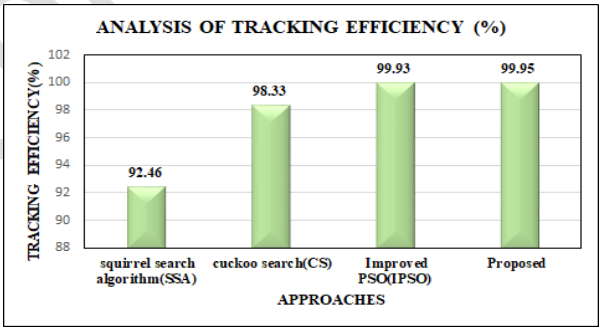

Fig. 20. Analysis of tracking efficiency

Uncorrected Proof

An analysis of tracking efficiency for SA [33], CS [34], IPSO [35] and WOA-RBFFIS MPPT approach is represented in Fig. 20. Here, the WOA-RBFFIS MPPT approach has the better tracking efficiency of 99.95% than other MPPT approaches, denoting the reliability of the system is enriched.

Table 2 Analysis of convergence time

Approaches	**Convergence time in s**
SA [33]	0.119
CS [34]	0.092
IPSO [35]	0.037
WOA-RBFFIS MPPT	**0.**035

The convergence time of WOA-RBFFIS MPPT is compared with SA [33], CS [34], IPSO [35] approaches, as depicted in Table 2. Thus, the WOA-RBFFIS MPPT has the lowest convergence time of 0.035s, indicating the dynamic efficacy is enhanced.

4. Conclusion

In this research, the PV system is integrated with high gain TWMGB converter and WOA based RBF-FIS MPPT controller. The Triple Winding Max Gain Boost converter efficiently enhances the PV voltage with maximum voltage gain and reduced component stress. Subsequently, the RBF-FIS MPPT assures accurate and quick tracking of the global maximum power point by dynamically tuning the parameters in response to real time environmental changes. Then, the exploitation of WOA enhances the learning efficiency of the RBFFIS, leading to better decision making and minimal steady state error. The coordinated operation among the converter and MPPT algorithm improves the dynamic response of system, diminishes oscillations and enhances efficacy. Simulation outcomes via the MATLAB/Simulink software demonstrates the converter efficacy of 97.61%, with enhanced voltage regulation, faster transient performance and enhanced tracking accuracy under changing temperature and irradiance conditions.

Uncorrected Proof

Furthermore, the converter offers minimal ripple and diminished switching losses, contributing to longer component lifespan and overall system reliability. This combined method assures maximum power extraction, effective voltage regulation and optimized energy delivery to the load. The system proves a robust and intelligent solution for next-generation PV applications, comprising standalone systems, DC microgrids and electric vehicle charging stations.

References

1. F. Blaabjerg, Y. Yang, K. A. Kim and J. Rodriguez, "Power Electronics Technology for Large-Scale Renewable Energy Generation," in Proceedings of the IEEE, vol. 111, no. 4, pp. 335-355, 2023.
2. P. Thirusenthil Kumaran, A. Vinayagam, S. T. Suganthi, "Veerasamy, Veerapandiyan; Inbamani, Abinaya; Chandran, Jaideep; Farade, Rizwan A; A voting approach of ensemble classifier for detection of power quality in islanded pv microgrid," IETE Journal of Research, vol. 69, no. 10, pp. 7408-7424, 2023, Taylor & Francis.
3. B. Modu, M. P. Abdullah, A. Alkassem, H. Z. Garni and M. Alkabi, "Optimal Design of a Grid-Independent Solar-Fuel Cell-Biomass Energy System Using an Enhanced Salp Swarm Algorithm Considering Rule-Based Energy Management Strategy," in IEEE Access, vol. 12, pp. 23914-23929, 2024.
4. M. F. Ali, M. R. Sheikh, A. A. Mamun and M. J. Hossen, "Techno-Economic, Predictive Modeling, and Demand Response Analysis of a Renewable Energy-Based Microgrid for Residential Applications," in IEEE Access, vol. 13, pp. 53748-53771, 2025.
5. N. C. Alluraiah and P. Vijayapriya, "Optimization, Design, and Feasibility Analysis of a Grid-Integrated Hybrid AC/DC Microgrid System for Rural Electrification," in IEEE Access, vol. 11, pp. 67013-67029, 2023.

Uncorrected Proof

6. M. M. Ahmed et al., "Mitigating Uncertainty Problems of Renewable Energy Resources Through Efficient Integration of Hybrid Solar PV/Wind Systems Into Power Networks," in IEEE Access, vol. 12, pp. 30311-30328, 2024.
7. A. Kumar, M. Alaraj, M. Rizwan and U. Nangia, "Novel AI Based Energy Management System for Smart Grid With RES Integration," in IEEE Access, vol. 9, pp. 162530-162542, 2021.
8. A. Inbamani, S. U. Prabha, "Predicting the Single Diode Model Parameters using Machine Learning Model," Electric Power Components and Systems, vol. 51, no. 14, pp. 1385-1397, 2023. Taylor & Francis.
9. A. Hayat, D. Sibtain, A. F. Murtaza, S. Shahzad, M. S. Jajja, and H. Kilic, "Design and analysis of input capacitor in DC–DC boost converter for photovoltaic-based systems," Sustainability, vol. 15, no. 7, pp. 6321, 2023.
10. N. Abouchabana, M. Haddadi, A. Rabhi, A. D. Grasso, and G. M. Tina, "Power efficiency improvement of a boost converter using a coupled inductor with a fuzzy logic controller: application to a photovoltaic system," Applied Sciences, vol. 11, no. 3, pp. 980, 2021.
11. A. S. Mansour, and M. S. Zaky, "A new extended single-switch high gain DC–DC boost converter for renewable energy applications," Scientific Reports, vol. 13, no. 1 264, 2023.
12. S. Pirpoor, S. Rahimpour, M. Andi, N. Kanagaraj, S.Pirouzi, and A. H. Mohammed, "A novel and high-gain switched-capacitor and switched-inductor-based DC/DC boost converter with low input current ripple and mitigated voltage stresses," IEEE Access, vol. 10, pp. 32782-32802, 2022.
13. H. Gholizadeh, S. A. Gorji, and D. Sera, "A quadratic buck-boost converter with continuous input and output currents," IEEE Access, vol. 11, pp. 22376-22393, 2023.
14. S. Danyali, R. Aazami, A. Moradkhani, and M. Haghi, "A new dual-input three-winding coupled-inductor based DC-DC boost converter for renewable energy applications," International Transactions on Electrical Energy Systems, vol. 31, no.1, pp. e12686, 2021.

Uncorrected Proof

15. S. Abbasian, M. Farsijani, H. S. Gohari, and T. Roinila, “Ultra-High Gain Quadratic DC-DC Topology Using Two-winding Coupled Inductors with Voltage Multiplier Cells,” IEEE Open Journal of Power Electronics, 2024.
16. Vaishnavi, Vishalakshi, A. Inbamani, “Perturb And Observe Algorithm Based MPPT Controller For A Stand-Alone Pv System Using Iot And Machine Learning Algorithms,” International Research Journal of Modernization in Engineering Technology and Science, 2021.
17. K. S. Kavin, P. S. Karuvelam, M. Matcha, and S. Vendoti, “Improved BRBFNN-based MPPT algorithm for coupled inductor KSK converter for sustainable PV system applications,” Electrical Engineering, pp. 1-23, 2025.
18. A. Inbamani, P. Umapathy, K. Chinnasamy, V. Veerasamy, S. V. Kumar, “Artificial intelligence and Internet of things for renewable energy systems,” vol.12, 2021, Walter de Gruyter GmbH & Co KG.'
19. K. Xia, Y. Li and B. Zhu, “Improved Photovoltaic MPPT Algorithm Based on Ant Colony Optimization and Fuzzy Logic Under Conditions of Partial Shading," in IEEE Access, vol. 12, pp. 44817-44825, 2024.
20. M. Saqib et al., “An Effective AFNIS-MPPT-Based Method for Optimizing Hybrid Energy Harvesting Systems,” in IEEE Access, vol. 13, pp. 45527-45543, 2025.
21. K. Paul Joshua, J. Mohanalin, and S. T. Jaya Christa, “Adaptive neuro-fuzzy inference system based under-frequency load shedding for Tamil Nadu,” The Journal of Supercomputing, vol. 76, no. 6, pp. 4184-4198, 2020.
22. A. O. Baatiah, A. M. Eltamaly, and M. A. Alotaibi, “Improving photovoltaic MPPT performance through PSO dynamic swarm size reduction,” Energies 16, no. 18, pp. 6433, 2023.
23. D. Mazumdar, P. K. Biswas, C. Sain, F. Ahmad, and L. Al-Fagih, “A robust MPPT framework based on GWO-ANFIS controller for grid-tied EV charging stations,” Scientific Reports, vol. 14, no. 1, pp. 30955, 2024.

Uncorrected Proof

24. R. B. Watanabe, O. H. Ando Junior, P. G. Martins Leandro, F. Salvadori, M. F. Beck, K. Pereira, M. H. Manzque Brandt, and F. M. de Oliveira, "Implementation of the bio-inspired metaheuristic firefly algorithm (FA) applied to maximum power point tracking of photovoltaic systems," Energies, vol. 15, no. 15, pp. 5338, 2022.
25. C. González-Castaño, C. Restrepo, S. Kouro, and J. Rodriguez, "MPPT algorithm based on artificial bee colony for PV system," Ieee Access, vol. 9, pp. 43121-43133, 2021.
26. E. Trojovská, M. Dehghani, and P. Trojovský, "Zebra optimization algorithm: A new bio-inspired optimization algorithm for solving optimization algorithm," Ieee Access, vol. 10, pp. 49445-49473, 2022.
27. P. Trojovský, and M. Dehghani, "Pelican optimization algorithm: A novel nature-inspired algorithm for engineering applications," Sensors, vol. 22, no. 3, pp. 855, 2022.
28. M. Karimi, H. Farzanehfard, M. Packnezhad, M. Esteki, "Bidirectional zvs buck-boost converter with single auxiliary switch and continuous current at low voltage source," IEEE Trans. Ind. Electron, vol. 69, no. 3, pp. 2480–2487, 2021.
29. M. Packnezhad, H. Farzanehfard, "Soft-switching high step-up/down converter using coupled inductors with minimum number of components," IEEE Trans. Ind. Electron, vol. 68, no. 9, pp. 7938–7945, 2021.
30. A. R. Akhormeh, K. Abbaszadeh, M. Moradzadeh, A. Shahirinia, "High-gain bidirectional quadratic dc–dc converter based on coupled induc tor with current ripple reduction capability," IEEE Trans. Ind. Electron. vol.68, no. 9, pp. 7826–7837, 2021.
31. H. Gholizadeh, S. A. Gorji, and D. Sera, "A quadratic buck–boost converter with continuous input and output currents," IEEE Access, vol. 11, pp. 22376–22393, 2023.
32. M. Okati, M. Eslami, M Jafari Shahbazzadeh and H. Shareef, "A new transformerless quadratic buck–boost converter with high voltage gain ratio and continuous input/output current port," IET Power Electron, vol. 15, no. 13, pp. 1280–1294, 2022.

Uncorrected Proof

33. D. Fares, M. Fathi, I. Shams, and S. Mekhilef. “A novel global MPPT technique based on squirrel search algorithm for PV module under partial shading conditions,” Energy Convers. Manag., vol. 230, pp. 113773, 2021.

34. A. A. Al-Shammaa, A. M. Abdurraqeeb, A. M. Noman, A. Alkuhayli, and H. M. H. Farh, “Hardware-In-the-loop validation of direct MPPT based cuckoo search optimization for partially shaded photovoltaic system,” Electronics, vol. 11, no. 10, pp. 1655, 2022.

35. C. B. Regaya, H. Hamdi, F. Farhani, A. Marai, A. Zaafouri, and A. Chaari, “Real-time implementation of a novel MPPT control based on the improved PSO algorithm using an adaptive factor selection strategy for photovoltaic systems,” ISA Trans., (2023).

Uncorrected Proof